Electrochemically activated MnO as a cathode material for sodium-ion batteries

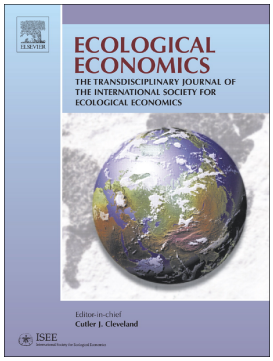

Electrochemically activated MnO as a cathode material for sodium-ion batteries

Leiting Zhang, Dmitry Batuk, Guohua Chen, Jean-Marie Tarascon

PII: S1388-2481(17)30061-9
DOI: doi: 10.1016/j.elecom.2017.02.020
Reference: ELECOM 5892

To appear in: *Electrochemistry Communications*

Received date: 9 February 2017
Revised date: 24 February 2017
Accepted date: 24 February 2017

Please cite this article as: Leiting Zhang, Dmitry Batuk, Guohua Chen, Jean-Marie Tarascon , Electrochemically activated MnO as a cathode material for sodium-ion batteries. The address for the corresponding author was captured as affiliation for all authors. Please check if appropriate. Elecom(2016), doi: 10.1016/j.elecom.2017.02.020

Electrochemically activated MnO as a cathode material for sodium-ion batteries

Leiting Zhang[a,b], Dmitry Batuk[a,c], Guohua Chen[b,d *], and Jean-Marie Tarascon[a,e,f *]

[a] Chimie du Solide et de l'Énergie, UMR 8260, Collège de France, 11 place Marcelin Berthelot, 75231 Paris Cedex 05, France

[b] Department of Chemical and Biomolecular Engineering, The Hong Kong University of Science and Technology, Clear Water Bay, Kowloon, Hong Kong

[c] EMAT, University of Antwerp, Groenenborgerlaan 171, B-2020 Antwerp, Belgium

[d] Department of Mechanical Engineering, The Hong Kong Polytechnic University, Hung Hom, Hong Kong

[e] Réseau sur le Stockage Électrochimique de l'Énergie (RS2E), FR CNRS 3459, 80039 Amiens, France

[f] Institute for Advanced Study, Visiting Professor of the Department of Chemical and Biomolecular Engineering, The Hong Kong University of Science and Technology, Clear Water Bay, Kowloon, Hong Kong

Email: guohua.chen@polyu.edu.hk, jean-marie.tarascon@college-de-france.fr

Abstract

Besides classical electrode materials pertaining to Li-ion batteries, recent interest has been devoted to pairs of active redox composites having a redox center and an intercalant source. Taking advantage of the $NaPF_6$ salt decomposition above 4.2 V, we extrapolate this concept to the electrochemical *in situ* preparation of F-based MnO composite electrodes for Na-ion batteries. Such electrodes exhibit a reversible discharge capacity of 145 mAh g^{-1} at room temperature. The amorphization of pristine MnO electrode after activation is attributed to the electrochemical grinding effect caused by substantial atomic migration and lattice strain build-up upon cycling.

Keywords: redox composites, *in situ* synthesis, electrolyte stability, oxyfluorides.

1. Introduction

Sodium-ion batteries (SIBs) are regaining great attention nowadays because of the abundance of Na in the Earth's crust [1]. Numerous Na-based compounds synthesized in recent years demonstrated promising results as cathode materials for SIBs [2,3]. However, the material design progress still falls behind the ever-increasing market demand, which calls for new materials with improved energy density. In the course of this expedition, a few groups beside us showed feasibility to trigger the electrochemical activity of a composite electrode consisting of metal oxide (MO) and lithium fluoride (LiF) in Li-ion batteries (LIBs) [4-7]. More specifically, within this new finely divided composite powders prepared by mechanical ball-milling, the transition metal serves as electron reservoir and LiF provides Li^+ ion to balance the charge. Such a combination of light constituents enables exceedingly high theoretical capacity over 250 mAh g^{-1} based on one electron transfer of common 3*d*-metals (Mn, Fe, etc.).

$$\mathrm{MO} + \mathrm{LiF} \leftrightarrow \mathrm{MOF} + \mathrm{Li}^+ + e^-$$

Although not fully understood, the proposed reaction scheme can be generalized to various transition metal oxides *via* eco-synthesis approaches, providing new insights into material design perspective. In the present work, we adopt this concept to SIBs by switching the fluorine source to NaF and using MnO as the redox component. We show that a MnO-0.1NaF composite prepared by high-energy ball-milling for 30 minutes delivers 157 mAh g^{-1} on the first discharge, and quickly stabilizes to 122 mAh g^{-1} on succeeding cycles in $NaPF_6$-based electrolyte. We further reveal that upon charging, the $NaPF_6$ partially decomposes above 4.2 V releasing NaF, which can act as an internal source of F^-, hence leading to *in situ* prepared electrodes with reversible capacity of 145 mAh g^{-1}.

2. Experimental

Commercial MnO (Sigma Aldrich, 99%) and NaF (Alfa Aesar, 99%) were used to prepare cathode composites. MnO-*x*NaF composites with various molar ratios (0, 0.1, 0.5, 1, and 1.5) were mixed in a stainless-steel vial of 10 mL with ball-to-powder ratio of 15. The vial was sealed in Ar and mounted in a SPEX high-energy ball mill adopting 875 cycles/minute 3D movement for 15 minutes. Then, 20 wt% of conductive C_{sp} was added and the composites were milled for another 15 minutes.

The structure of as-prepared composites was examined by X-ray diffraction (XRD) using a Bruker D8 advance diffractometer equipped a Cu source ($\lambda_{Cu\,K\alpha1} = 1.54056$ Å, $\lambda_{Cu\,K\alpha2} = 1.54439$ Å) and a LynxEye detector. Particle morphology was analyzed using scanning electron microscopy (SEM) and high angle annular dark field scanning transmission electron microscopy (HAADF-STEM). The elemental distribution was analyzed with energy-dispersive X-ray spectroscopy acquired in STEM mode (STEM-EDX). Together with XRD, the crystallinity of the composites was examined using electron diffraction (ED). The SEM images were recorded on an FEI Helios NanoLab 650 instrument, and the TEM data were collected on an FEI Tecnai Osiris microscope equipped with a Super-X detector.

The electrochemical activity of composites was assessed in the Swagelok-type cells, using some 12 mg of MnO-xNaF/Csp composite as the cathode, sodium metal as the anode, some 250 µL of 1 mol L-1 of NaPF6 in EC/DMC (1/1 vol%, 1.3 g cm^{-3}) as the electrolyte, and 3 layers of Whatman GF/D glassfiber as the separator. Cells were cycled in galvanostatic mode between 4.5-1.2 V at room temperature under a current density of 5 mA g^{-1}.

3. Results and discussion

Fig. 1a demonstrates a typical XRD pattern of the MnO-*x*NaF composites prepared by ball-milling for 30 minutes. The pattern shows broadening of the Bragg peaks pertaining to MnO, indicating reduced particle size and increased lattice strain. Peaks corresponding to NaF, added in small amounts to the composite, are also visible in the profile. This indicates that the ball milling does not trigger chemical reaction between components, which is also confirmed by the SEM (Fig. 1b) and STEM-EDX (Fig. 1c) data. The MnO-*x*NaF composites contain relatively large MnO and NaF particles of irregular shape (ranging from a few tens to several hundred nanometers) intimately mixed with uniform carbon nanoparticles of a few tens of nanometers in size.

The prepared composites were cycled in Na half cells, and the results are summarized in Fig. 2. During the first charge, a typical voltage composition curve shows a long plateau at 4.3 V, which disappears on the following discharge and does not reappear on subsequent cycles, so that it can be viewed as the formation cycle. While all MnO-*x*NaF samples show good capacity retention over the first ten cycles, the MnO-0.1NaF composite delivers the highest first cycle discharge capacity of 157 mAh g^{-1} and a sustainable capacity retention of 122 mAh g^{-1} (Fig. 2a) corresponding to ~0.5 e^- transfer per MnO unit formula. When replacing the electrolyte salt by a non-fluorinated one, *i.e.* $NaClO_4$, the same composite delivers less than 80 mAh g^{-1} capacity, indicating that the F-rich environment proactively provides F to facilitate the MnO activation. On the other hand, increasing the NaF content decreases the overall capacity (Fig. 2b), and this effect is most likely nested in the insulating nature of NaF.

Such F-driven activation of binary oxides was reported earlier by Jung *et al.* but the importance of the F content with respect to Mn was never mentioned [6]. We have previously demonstrated the significance of this factor for MnO-LiF composites; and

our present data for the MnO-NaF composites further confirm the participation of the F-based salt in the reaction processes. Thus, we decided to examine the impact of $NaPF_6$, bearing in mind the following electrolyte equilibrium: $[PF_6^- \leftrightarrow PF_5 + F^-]$ [8]. We directly cycled a F-free MnO electrode in $NaPF_6$ electrolyte and obtained a capacity of only 12 mAh g^{-1} with the absence of the first cycle activation plateau. Interestingly, the capacity builds up upon cycling and stabilizes at 145 mAh g^{-1} (Fig. 2c-d). Such a stepwise activation based on trace decomposition of $NaPF_6$ in each cycle is distinct from the one-step activation observed for the MnO-0.1NaF composite. This further proves that the ball-milling step together with the addition of external fluorine source is useful but not essential to trigger the electrochemical activity of MnO in $NaPF_6$ electrolyte. Moreover, we confirm that this long activation step can be significantly shortened by cycling the cell at 55 °C, thanks to the drastic decomposition of $NaPF_6$ at this temperature. The resulting voltage-composition data agree with our previous study in Li-ion system with 200-300 mV shifts in voltage [5].

The performance of the MnO-*x*NaF cathodes can be compared to that of the MnO-*x*LiF composites. Both systems demonstrate the feasibility of activating MnO electrode with good reversible capacity. The alkaline metal fluorides AF (A = Li, Na, *etc.*) serve as initiators to trigger the MnO oxidation via electrochemically splitting of the A-F bond [7]. Thereafter, the decomposition of APF_6 salts becomes easily accessible to sustain the oxidation process. In the absence of starting AF, MnO only reacts with trace amount of F^- liberated from the electrolyte after each oxidation. The direct defluorination of $NaPF_6$ has much higher energy barrier, which can be triggered by elevating the cycling temperature. Besides, it is worth mentioning that the Coulombic efficiency is only 60% for the first cycle and approaches 90% in the following cycles, implying continuous parasitic electrolyte degradation on both electrodes. Our previous work on the MnO-LiF/$LiPF_6$/Li system shows respective values of 75% and 92% [5]. The huge difference in the first cycle mainly nested on the Na anode that is the source of drastic electrolyte reduction during the formation

cycle [9]. Currently, we are examining the full cell performance of the composite, hoping to tackle this issue by replacing Na with less reactive Sb-based alloy anodes [10].

To get more insight in the processes associated with the electrochemical activity of the composites, we monitored the evolution of their crystal structure. XRD data demonstrate progressive loss of the electrode crystallinity upon activation as witnessed by the presence of weak and extremely broadened Bragg peaks for the oxidized electrodes. The HAADF-STEM image reveals numerous cracks in the particles (Fig. 3), which are indicative of an electrochemically-driven grinding process. The ED data together with radially integrated diffraction patterns demonstrate a dramatic structural transformation of the material upon first oxidation, with namely broadening of ED spots and the appearance of new ones. These results suggest that the activation of the MnO-*x*NaF composites is associated with a substantial atomic migration in the parent rocksalt MnO structure. It leads to the fragmentation of the material into tiny domains (of mere nanometers) with a new atomic arrangement and induces strong elastic strain. Therefore, the poor quality of the data prevents a precise analysis of the resulting structure. Lastly, STEM-EDX analysis indicates a uniform distribution of F across the particles of the activated MnO-*x*NaF composites; however minor variation can be hidden by the overlap of the Mn-L and F-K emission lines. We are now employing various bulk- and surface-sensitive techniques to unveil the details of the structure and Mn oxidation state transformations in the composites.

4. Conclusions

In conclusion, we have successfully generalized the redox composite model derived from lithium-ion to sodium-ion batteries. High-energy ball-milling as short as

30 minutes is sufficient to prepare reproducible and easily scalable MnO-*x*NaF composites. A reversible capacity of 122 mAh g^{-1} is achieved by cycling MnO-0.1NaF in half cells. It can be further improved to 145 mAh g^{-1} using $NaPF_6$ as the sole F-source at the expense of a lengthy activation process and partial consumption of the electrolyte salt. While the practical aspect of such *in situ*-prepared electrodes remain to be proven, we must emphasize that this electrochemically-driven synthesis process opens a new door to novel Li(Na)-based electrode materials as preliminary results with other 3*d*-metals seem to indicate.

Acknowledgements

This research did not receive any specific grant from funding agencies in the public, commercial, or not-for-profit sectors. L.Z. thanks the HKUST for his Postgraduate Studentship.

Figures

Fig. 1 (a) XRD profile of MnO-0.1NaF composite compared to that of pristine MnO, note the broadening of the reflections as a result of ball-milling; (b) SEM image of MnO-0.1NaF composite showing that large MnO and NaF particles of varying shapes and sizes are intimately mixed with C_{sp} particles; (c) typical STEM-EDX data for the MnO-0.1NaF composite, showing that after ball-milling MnO and NaF are present in the sample as separate particles.

Fig. 2 (a) One-step activation of MnO-0.1NaF composite in $NaPF_6$ electrolyte; (b) cycling behavior of MnO-*x*NaF (*x* = 0, 0.1, 0.5, 1, 1.5) in $NaPF_6$ electrolyte and MnO-0.1NaF in $NaClO_4$ electrolyte; (c) stepwise activation of MnO electrode in $NaPF_6$ electrolyte; and (d) the corresponding cycling behavior.

Fig. 3 TEM images for the pristine and activated MnO-0.1NaF composites. The HAADF-STEM images compare the morphology of the particles, highlighting the formation of numerous cracks in individual MnO particles (top). The ED patterns (middle) and the corresponding radially integrated intensity profiles (bottom) demonstrate dramatic structure transformation on the first oxidation step.

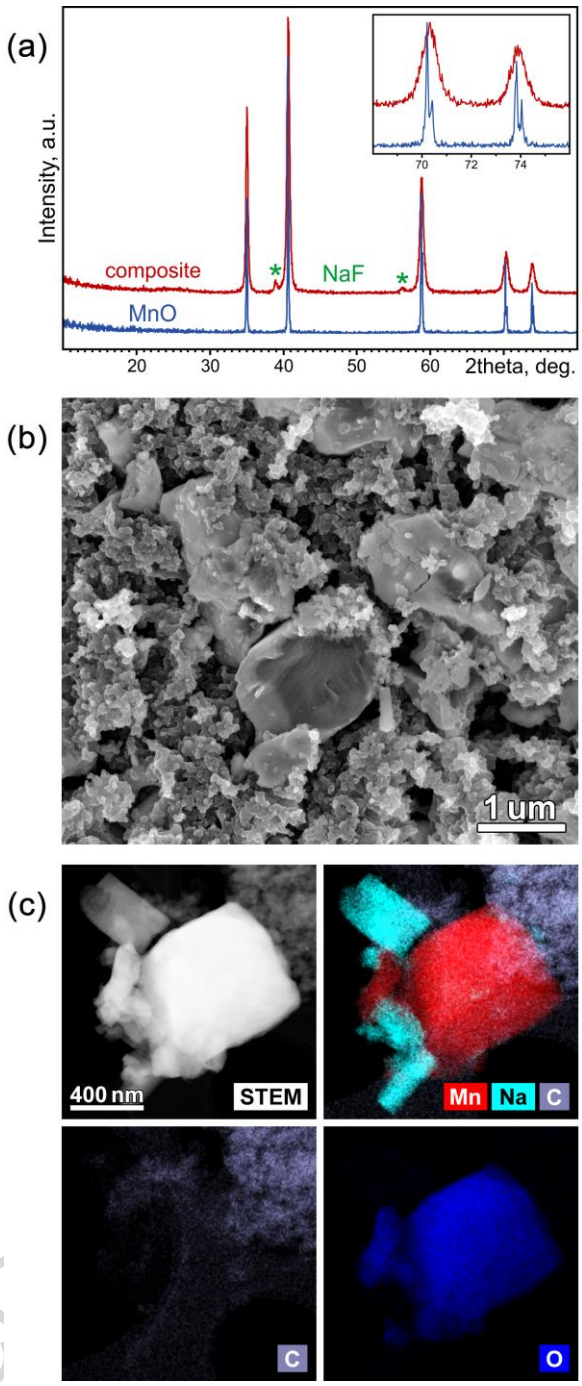

Fig. 1

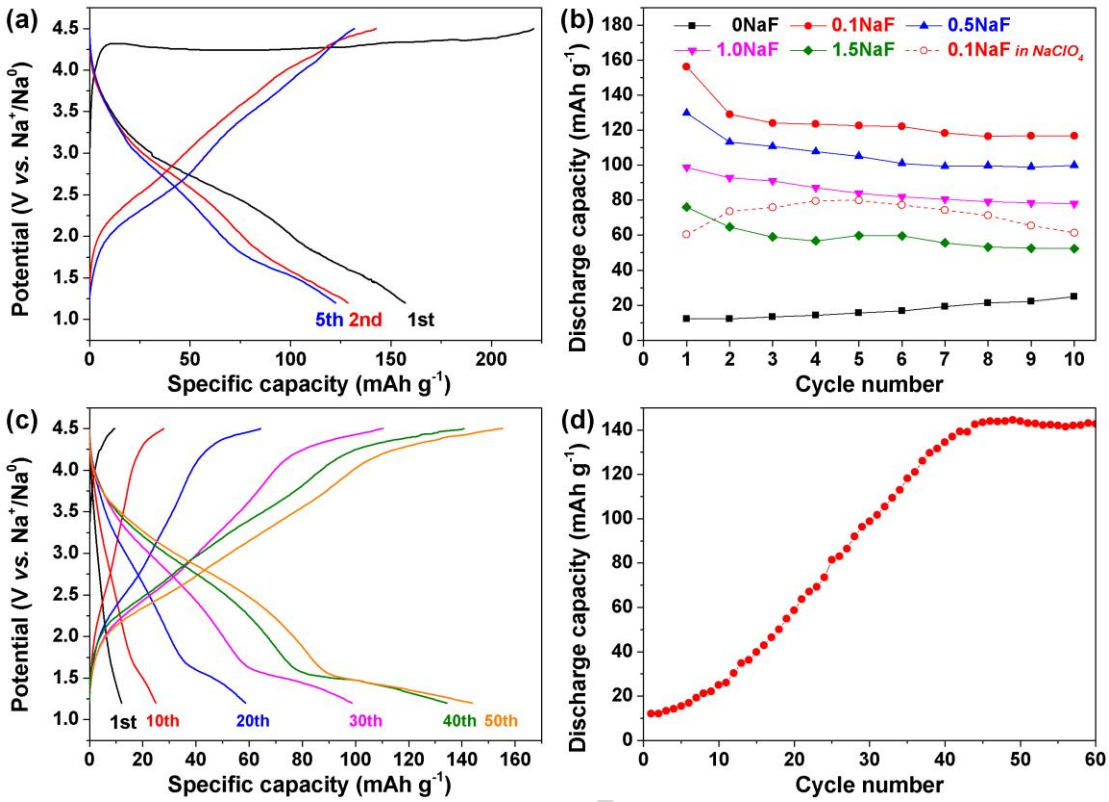

Fig. 2

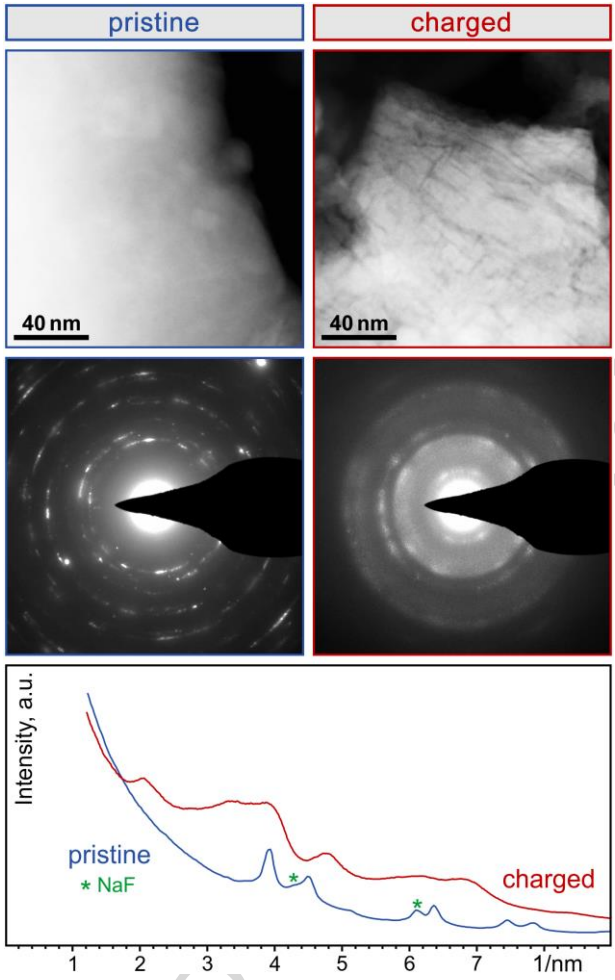

Fig. 3

References

[1] N. Yabuuchi, K. Kubota, M. Dahbi, S. Komaba, Research development on sodium-ion batteries, Chem. Rev. 114 (2014) 11636–11682. doi:10.1021/cr500192f.

[2] S.-W. Kim, D.-H. Seo, X. Ma, G. Ceder, K. Kang, Electrode materials for rechargeable sodium-ion batteries: potential alternatives to current lithium-ion batteries, Adv. Energy Mater. 2 (2012) 710–721. doi:10.1002/aenm.201200026.

[3] V. Palomares, P. Serras, I. Villaluenga, K.B. Hueso, J. Carretero-González, T. Rojo, Na-ion batteries, recent advances and present challenges to become low cost energy storage systems, Energy Environ. Sci. 5 (2012) 5884–18. doi:10.1039/c2ee02781j.

[4] S.-W. Kim, K.-W. Nam, D.-H. Seo, J. Hong, H. Kim, H. Gwon, et al., Energy storage in composites of a redox couple host and a lithium ion host, Nano Today. 7 (2012) 168–173. doi:10.1016/j.nantod.2012.04.004.

[5] L. Zhang, G. Chen, E.J. Berg, J.M. Tarascon, Triggering the in situ electrochemical formation of high capacity cathode material from MnO, Adv. Energy Mater. (2016). doi:10.1002/aenm.201602200.

[6] S.-K. Jung, H. Kim, M.G. Cho, S.-P. Cho, B. Lee, H. Kim, et al., Lithium-free transition metal monoxides for positive electrodes in lithium-ion batteries, Nat. Energy. 2 (2017) 16208.

[7] N. Dimov, A. Kitajou, H. Hori, E. Kobayashi, S. Okada, Electrochemical splitting of LiF: a new approach to lithium-ion battery materials, ECS Transactions. 58 (2014) 87–99. doi:10.1149/05812.0087ecst.

[8] K. Tasaki, K. Kanda, S. Nakamura, M. Ue, Decomposition of $LiPF_6$ and stability of PF_5 in Li-ion battery electrolytes, J. Electrochem. Soc. 150 (2003) A1628–A1636. doi:10.1149/1.1622406.

[9] D.I. Iermakova, R. Dugas, M.R. Palacin, A. Ponrouch, On the comparative stability of Li and Na metal anode interfaces in conventional alkyl carbonate electrolytes, J. Electrochem. Soc. 162 (2015) A7060–A7066. doi:10.1149/2.0091513jes.

[10] Y. Zhu, X. Han, Y. Xu, Y. Liu, S. Zheng, K. Xu, et al., Electrospun Sb/C fibers for a stable and fast sodium-ion battery anode, ACS Nano. 7 (2013) 6378–6386. doi:10.1021/nn4025674.

Highlights

- Manganese-based redox composite model is validated in sodium-ion batteries.
- MnO can be directly used as cathode material having 145 mAh g^{-1} reversible capacity in $NaPF_6$ electrolyte.
- The electrochemical activity of MnO in $NaPF_6$ electrolyte resides in catalytic decomposition of electrolyte salt upon oxidation.